cosmetics

MDPI

Article

Development and Optimization of a Quercetin-Loaded Chitosan Lactate Nanoparticle Hydrogel with Antioxidant and Antibacterial Properties for Topical Skin Applications

Raghda Yazidi [1], Majdi Hammami [1], Hamza Ghadhoumi [1], Ameni Ben Abdennebi [1], Sawssen Selmi [1], Kamel Zayani [2], Karima Horchani-Naifer [2], Iness Bettaieb Rebey [1,*] and Moufida Saidani Tounsi [1]

[1] Laboratory of Aromatic and Medicinal Plants, Borj Cedria Biotechnology Center, BP. 901, Hammam-Lif 2050, Tunisia; raghda.yazidi@cbbc.rnrt.tn (R.Y.); majdi.hammami@cbbc.rnrt.tn (M.H.); hamza.gadhoumi@cbbc.rnrt.tn (H.G.); benabdennebiameni9@gmail.com (A.B.A.); selmisawsencbbc@gmail.com (S.S.); moufida.saidani@cbbc.rnrt.tn (M.S.T.)

[2] Laboratory of Physico-Chemistry of Mineral Materials and Their Applications, National Center for Research in Materials Sciences CNRSM, Technopole Borj Cedria, BP. 73, Soliman 8027, Tunisia; kamel.zayani@cnrsm.rnrt.tn (K.Z.); karima_horchani@yahoo.com (K.H.-N.)

* Correspondence: ines.bettaieb@cbbc.rnrt.tn

Abstract

Nanotechnology has revolutionized dermocosmetic innovation by improving the stability, bioavailability, and efficacy of active ingredients. In this study, we developed and optimized a novel xanthan gum-based hydrogel containing quercetin-loaded chitosan lactate nanoparticles for antioxidant and antimicrobial skincare applications. Chitosan was converted to its lactate form to enhance water solubility and enable nanoparticle formation at physiological pH via ionic gelation with citric acid. The formulation was optimized using Box–Behnken response surface methodology to achieve minimal particle size and maximal zeta potential. The final gel was structured with xanthan gum as the gelling polymer, into which the optimized nanoparticles were incorporated to create a stable and bioactive hydrogel system. Encapsulation efficiency was measured separately to assess the effectiveness of drug loading. The optimized nanoparticles exhibited a mean diameter of 422.02 nm, a zeta potential of +29.49 mV, and a high quercetin encapsulation efficiency (76.9%), corresponding to the proportion of quercetin retained in the nanoparticle matrix relative to the total amount initially used in the formulation. Antioxidant assays (TAC, DPPH, and reducing power) confirmed superior radical-scavenging activity of the nanoformulation compared to the base hydrogel. Antibacterial tests showed strong inhibition against *Escherichia coli*, *Pseudomonas aeruginosa*, and *Staphylococcus aureus*, with MIC values comparable to streptomycin. Accelerated stability studies demonstrated excellent physicochemical and microbiological stability over 60 days. This natural, bioactive, and eco-friendly formulation represents a promising platform for next-generation cosmeceuticals targeting oxidative stress and skin-related pathogens.

Keywords: nanotechnology; chitosan lactate; quercetin nanoparticles; dermocosmetics; antioxidant; antibacterial; skin care; hydrogel

Academic Editor: Enzo Berardesca

Received: 15 May 2025
Revised: 28 June 2025
Accepted: 1 July 2025
Published: 3 July 2025

Citation: Yazidi, R.; Hammami, M.; Ghadhoumi, H.; Ben Abdennebi, A.; Selmi, S.; Zayani, K.; Horchani-Naifer, K.; Bettaieb Rebey, I.; Saidani Tounsi, M. Development and Optimization of a Quercetin-Loaded Chitosan Lactate Nanoparticle Hydrogel with Antioxidant and Antibacterial Properties for Topical Skin Applications. *Cosmetics* **2025**, *12*, 141. https://doi.org/10.3390/cosmetics12040141

1. Introduction

Nanotechnology has emerged as a pivotal innovation in the cosmetics industry, offering enhanced delivery systems for active compounds, improved stability, and increased efficacy of formulations [1]. Among various nanosystems, nanoparticles based on natural

biopolymers such as chitosan have gained increasing attention due to their biocompatibility, biodegradability, and ability to encapsulate bioactive molecules [2]. Chitosan, a cationic polysaccharide derived from the deacetylation of chitin, has been widely studied for its antimicrobial, antioxidant, and film-forming properties, making it highly suitable for cosmetic and dermatological applications [3]. Despite its advantages, chitosan exhibits limited water solubility at neutral pH, restricting its utility in certain topical formulations. To address this, chemical modifications such as the formation of chitosan salts (e.g., chitosan lactate) have been employed to enhance solubility and functional performance [4]. Chitosan lactate, prepared via reaction with lactic acid, retains the desirable bioactivities of native chitosan while exhibiting improved aqueous solubility and enhanced stability under physiological conditions [5]. These properties allow it to act as an effective nanocarrier for hydrophobic antioxidants and polyphenols.

Quercetin, a naturally occurring flavonol found in various fruits and vegetables, is well recognized for its potent antioxidant, anti-inflammatory, and anti-aging properties [6,7]. However, its poor water solubility and chemical instability limit its topical bioavailability and hinder its incorporation into conventional cosmetic formulations [8]. Despite its intrinsic chemical stability, quercetin is poorly soluble and prone to oxidative degradation in aqueous or physiological conditions, limiting its efficacy in topical formulations. To overcome these limitations, the encapsulation of quercetin in biopolymeric nanoparticles such as those based on chitosan derivatives has been proposed as a viable strategy to enhance its solubility, stability, and controlled release [9].

Encapsulating quercetin within chitosan lactate nanoparticles allows for the formation of a stable colloidal system that can be further incorporated into cosmetic creams or gels for enhanced dermal delivery. Nanoparticles can enhance skin penetration, prolong the residence time of active compounds on the skin, and protect sensitive ingredients from environmental degradation [10]. Moreover, the use of natural and biodegradable polymers aligns with the growing consumer demand for eco-friendly and sustainable cosmetic products [11].

Numerous studies have reported the use of chitosan-based nanoparticles in cosmetics for the delivery of antioxidants, antimicrobials, and anti-aging agents. For instance, chitosan nanoparticles have been used to deliver vitamins C and E, resveratrol, and other polyphenols to improve skin hydration and reduce oxidative stress [12–14]. The incorporation of quercetin-loaded nanoparticles into a hydrogel matrix further enhances formulation stability, user acceptability, and ease of application. Xanthan gum is commonly employed as a gelling agent in such systems due to its non-toxic, biocompatible, and rheologically favorable properties [15].

Response surface methodology (RSM) has become a standard statistical tool for optimizing nanoparticle formulations. It allows for the systematic assessment of key formulation variables such as polymer concentration, crosslinker type, and active compound loading, facilitating the development of formulations with desired particle size, zeta potential, and encapsulation efficiency [16]. Smaller particle size is generally correlated with better skin penetration and higher surface area, whereas an optimal zeta potential (typically $> |30|$ mV) ensures colloidal stability and prevents aggregation [17].

The present study focuses on the preparation and characterization of chitosan lactate/quercetin nanoparticles, their incorporation into a xanthan gum-based gel, and the evaluation of their physicochemical, antioxidant, and antimicrobial properties for potential cosmetic applications. We hypothesize that encapsulating quercetin in chitosan lactate nanoparticles will enhance its solubility and efficacy, while the hydrogel matrix will provide a stable and user-friendly platform for topical application. In addition to evaluating the *in vitro* antioxidant and antibacterial activities of the nanoparticles and final hydrogel

formulation, this work also addresses stability under accelerated storage conditions—a critical parameter for cosmetic product development. The antimicrobial activity, particularly against skin-associated pathogens such as *Staphylococcus aureus* and *Pseudomonas aeruginosa*, was also assessed, as these microorganisms are frequently implicated in cosmetic product contamination and dermatological infections [18].

To the best of our knowledge, this is the first study to report the formulation of chitosan lactate–quercetin nanoparticles incorporated into a xanthan gum-based hydrogel for dermal use. This dual system enhances the solubility of both chitosan and quercetin, while ensuring gel stability and topical applicability. This natural, bioactive, and eco-friendly formulation represents a promising platform for next-generation cosmeceuticals targeting oxidative stress and skin-related pathogens, with enhanced storage stability compared to the base hydrogel.

2. Materials and Methods

2.1. Materials

Quercetin dihydrate (≥95%) (Figure 1), lactic acid, citric acid monohydrate, ethanol (≥99.5%), acetic acid, sodium hydroxide, formic acid, Mueller–Hinton broth, nutrient agar, resazurin, and all solvents used in this study were of analytical grade and obtained from Sigma-Aldrich (St. Louis, MO, USA). Chitosan (medium molecular weight, degree of deacetylation ≥ 90%) was provided by Chitelix S.A. (Bizerte, Tunisia) and used as received without further purification. Xanthan gum (pharmaceutical grade, Sigma-Aldrich, St. Louis, MO, USA) was employed as the gelling agent in hydrogel preparation. Cosgard® (a commercial preservative composed of phenoxyethanol and ethylhexylglycerin) was obtained from Aroma-Zone (Lyon, France).

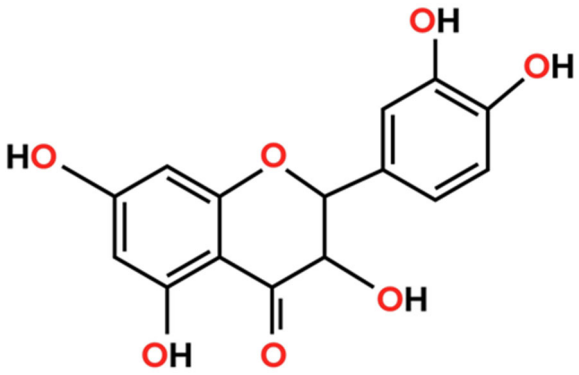

Figure 1. Quercetin chemical structure.

2.2. Chitosan Characterization

Chitosan used in this study was characterized for its degree of deacetylation (DD), molecular weight, viscosity, and ash content. The DD was determined using two complementary methods: Fourier Transform Infrared Spectroscopy (FTIR) and a potentiometric titration assay. For FTIR, spectra were recorded in the range of 4000–400 cm^{-1}, and the DD was calculated based on the absorbance ratio of specific functional groups according to Baxter et al. [19]. In parallel, a potentiometric method was employed for independent confirmation [20]. The molecular weight of chitosan was estimated by viscometric analysis. A 1% (*w*/*v*) chitosan solution was prepared in 1% (*v*/*v*) acetic acid and stirred for 24 h at room temperature [21]. The viscosity was measured at 25 ± 1 °C using a PCE-RVI 2 digital rotational viscometer (PCE Instruments, Meschede, Germany), equipped with appropriate spindle and rotation speed as recommended by the manufacturer. The viscosity values were recorded in centipoise (cP), and the average molecular weight was estimated using the

Mark–Houwink equation [22]. Each measurement was performed in triplicate. Ash content was determined by incinerating a known quantity of dry chitosan in a muffle furnace at 510 °C for 6 h, and the residue was weighed to calculate the mineral content as a percentage of the original mass.

2.3. Preparation of Chitosan Lactate

Chitosan lactate was prepared following the method described by Weecharangsan et al. [4], with slight modifications. Briefly, 6 g of chitosan powder was dissolved in 200 mL of 3% (*w*/*v*) lactic acid solution under constant magnetic stirring at 60 °C for 6 h. The resulting homogenous viscous solution was frozen at −20 °C and subsequently lyophilized to obtain a dry, amorphous powder. The freeze-dried product was then finely ground using a mortar and pestle and stored in airtight containers at room temperature until further use.

2.4. Chitosan Lactate and Hydrogel Characterization

2.4.1. FTIR Spectral Analysis

The structural properties of chitosan lactate were examined by Fourier Transform Infrared Spectroscopy (FTIR). The spectrum was recorded within the 4000–400 cm^{-1} range using a 100 FTIR spectrometer (Perkin-Elmer Inc., Norwalk, CT, USA). Key functional groups corresponding to the polysaccharide backbone and lactate modifications were identified and analyzed to confirm successful derivatization and assess structural integrity.

2.4.2. Antioxidant Activity Assays

To comprehensively evaluate the antioxidant potential of chitosan lactate, three complementary *in vitro* assays were employed: total antioxidant capacity (TAC), DPPH radical scavenging activity, and ferric reducing power. All assays were conducted in triplicate, and results were expressed as mean ± standard deviation.

- Total Antioxidant Capacity (TAC)

The phosphomolybdenum method was used to assess TAC, based on the reduction of Mo(VI) to Mo(V) under acidic conditions, forming a green phosphate/Mo(V) complex measurable at 695 nm, as described by Prieto et al. [23]. Briefly, 100 µL of sample was mixed with 1 mL of reagent solution composed of sulfuric acid (0.6 N), sodium phosphate (28 mM), and ammonium molybdate (4 mM). The tubes were incubated at 95 °C for 90 min, then cooled to room temperature. Absorbance was measured against a blank containing methanol instead of the sample. TAC values were expressed as mg gallic acid equivalents per gram of dry matter (mg GAE/g DM), using a gallic acid standard curve.

- DPPH Radical Scavenging Activity

Antiradical activity was evaluated using the stable 2,2-diphenyl-1-picrylhydrazyl (DPPH) radical as described by Rguez et al. [24]. A total of 1 mL of the extract at various concentrations was added to 250 µL of DPPH solution (0.2 mM in methanol). The reaction mixture was incubated in the dark for 30 min at room temperature, and the absorbance was recorded at 517 nm against a blank (methanol + DPPH). The percentage of inhibition was calculated using the formula:

$$\%\text{Inhibition} = ((A_{control} - A_{sample})/A_{control}) \times 100 \quad (1)$$

where $A_{control}$ is the absorbance of the control (DPPH solution without sample) and A_{sample} is the absorbance in the presence of chitosan lactate. All measurements were performed in triplicate.

- Ferric Reducing Power

The ability of chitosan lactate to reduce Fe^{3+} to Fe^{2+} was assessed according to the method of Oyaizu [25], with slight modifications. A volume of 1 mL of sample was mixed with 2.5 mL of phosphate buffer (0.2 M, pH 6.6) and 2.5 mL of potassium ferricyanide (1%, *w*/*v*). After incubation at 50 °C for 20 min, 2.5 mL of trichloroacetic acid (10%, *w*/*v*) was added to stop the reaction. The mixture was centrifuged at 650× *g* for 10 min, and 2.5 mL of the supernatant was mixed with 2.5 mL of distilled water and 0.5 mL of ferric chloride (0.1%, *w*/*v*). Absorbance was measured at 700 nm. The EC_{50} value was defined as the sample concentration corresponding to an absorbance of 0.5, indicating half-maximal reducing power. All antioxidant tests were conducted in triplicate to ensure reproducibility.

2.4.3. Antibacterial Activity Assessment

The minimum inhibitory concentration (MIC) and minimum bactericidal concentration (MBC) of chitosan lactate nanoparticles were assessed using the standard broth microdilution method in sterile 96-well microtiter plates, following CLSI guidelines and with modifications based on Duarte et al. [26]. Mueller–Hinton broth (MHB) was used as the growth medium. A standardized bacterial inoculum was prepared for each tested strain (*Escherichia coli* and *Pseudomonas aeruginosa*), adjusted to a turbidity equivalent to 0.5 McFarland standard (~1.5 × 10^8 CFU/mL), and further diluted to reach approximately 10^6 CFU/mL in the assay wells. Each well was filled with 100 µL of MHB containing varying concentrations of chitosan lactate nanoparticles (ranging from 10 to 50 µg/mL), along with 10 µL of resazurin solution (0.015%) as a redox-sensitive viability indicator. A 100 µL aliquot of the bacterial suspension was added to each well to achieve a final volume of 200 µL. Negative controls (MHB only), positive controls (MHB + bacteria), and solvent controls were included in each plate. The plates were sealed and incubated at 37 °C for 18 to 24 h under static conditions. MIC was visually determined as the lowest concentration of nanoparticles at which no color change of resazurin (from blue to pink) was observed, indicating complete inhibition of bacterial metabolic activity. For MBC determination, 10 µL from each well that showed no visible color change were aseptically plated onto nutrient agar and incubated at 37 °C for an additional 24 h. The MBC was defined as the lowest concentration of chitosan lactate nanoparticles that resulted in no colony formation, corresponding to ≥99.9% bacterial death. All tests were performed in triplicate and repeated in two independent experiments to ensure reproducibility. Results were expressed in µg/mL for both MIC and MBC values, and comparisons between bacterial strains were made to assess the spectrum of antibacterial efficacy [27].

2.5. Statistical Design and Optimization of Chitosan Lactate Nanoparticles

Chitosan lactate nanoparticles were prepared by the ionic gelation method [28]. Briefly, a predetermined amount of chitosan lactate was dissolved in deionized water under gentle magnetic stirring until complete solubilization. Separately, quercetin was dissolved in a minimal volume of ethanol to enhance dispersion and then slowly added to the chitosan solution. Citric acid, acting as a natural cross-linking agent, was dissolved in water and added dropwise to the mixture under continuous stirring at room temperature. The addition of citric acid induced immediate ionic cross-linking between the positively charged amino groups of chitosan and the negatively charged carboxyl groups of citric acid, leading to spontaneous nanoparticle formation.

Lyophilization of the resulting nanoparticle suspension was then performed using a Christ Alpha 2-4 LD Plus freeze dryer (Martin Christ, Osterode am Harz, Germany). Samples were pre-frozen at −20 °C for 12 h, followed by freeze-drying at −50 °C under a vacuum pressure of 0.01 mbar for 48 h. This process was applied to enhance the storage stability of the nanoparticles and facilitate accurate quantification in subsequent

formulation steps. Encapsulation efficiency was determined immediately after nanoparticle synthesis, prior to lyophilization, to avoid potential degradation or loss of unencapsulated quercetin during freeze-drying. In contrast, drug content was evaluated from the lyophilized nanoparticle powder to ensure consistency in final dosage calculations.

The formulation of chitosan lactate nanoparticles was optimized using a Box–Behnken experimental design, implemented through NemrodW software (LPRAI, version 2000) [29]. This statistical approach was applied to evaluate the effects and interactions of three independent variables: chitosan concentration (X_1, % m/v), quercetin concentration (X_2, mg/mL), and citric acid concentration (X_3, % m/v). The experimental domain was defined with central values of 2% for chitosan, 10 mg/mL for quercetin, and 2% for citric acid, each varied by a step of ± 1, ± 5, and ± 1 respectively. A total of 17 experimental runs were conducted, allowing for the estimation of 10 regression coefficients in the second-order polynomial model:

$$Y = b_0 + b_1X_1 + b_2X_2 + b_3X_3 + b_{11}{X_1}^2 + b_{22}{X_2}^2 + b_{33}{X_3}^2 + b_{12}X_1X_2 + b_{13}X_1X_3 + b_{23}X_2X_3 \quad (2)$$

Dynamic light scattering (DLS) was employed to assess the hydrodynamic diameter and zeta potential of the nanoparticles using a Zetasizer Nano ZS (Malvern Instrument Grovewood, UK). Prior to measurement, samples were diluted at a ratio of 1:10 in deionized water to minimize multiple scattering effects. Measurements were performed at 25 °C with a fixed backscattering angle of 173°. Zeta potential values were calculated from the electrophoretic mobility using the Smoluchowski approximation. Subsequently, a response surface model was established to optimize two critical quality attributes: nanoparticle size (Y_{size}, in nm) and zeta potential (Y_{zeta}, in mV), both of which are key indicators of colloidal stability and functional performance in biological applications. The design allowed a systematic evaluation of formulation variables and facilitated the identification of optimal synthesis conditions for the quercetin-loaded chitosan lactate nanoparticles The model was constructed to optimize two dependent responses: nanoparticle size (Y_{size}, in nm) and zeta potential (Y_{zeta}, in mV), which are critical parameters for assessing colloidal stability and biological performance. This design enabled an efficient exploration of the formulation space and facilitated the identification of optimal conditions for nanoparticle synthesis.

2.6. HPLC Quantification of Quercetin in Chitosan Lactate Nanoparticle and Hydrogel

The quantification of quercetin content in chitosan lactate nanoparticles and hydrogel was performed using high-performance liquid chromatography (HPLC). Sample preparation involved centrifugation of the nanoparticle suspension at 10,000 rpm for 20 min to recover the supernatant containing non-encapsulated quercetin, while a portion of the lyophilized nanoparticles was dissolved in an appropriate solvent for total quercetin determination [30]. HPLC analyses were conducted using an Agilent 1260 Infinity system (Agilent Technologies, Waldbronn, Germany) equipped with a quaternary pump and a photodiode array detector. Separation was carried out on a Zorbax Eclipse XDB-C18 reversed-phase column (100 × 4.6 mm, 5 µm), maintained at 25 °C. The mobile phase consisted of solvent A (HPLC-grade water with 0.1% formic acid) and solvent B (acetonitrile), delivered at a constant flow rate of 0.7 mL/min. The gradient program was as follows: 90% A/10% B from 0 to 40 min, 50% A/50% B from 40 to 41 min, 100% B from 41 to 50 min, and return to 90% A/10% B from 50 to 59 min. The injection volume was 3 µL, and quercetin was detected at 280 nm. Quantification was based on calibration curves of standard quercetin solutions ranging from 10 to 1000 µg/mL, and results were expressed in mg quercetin per gram of extract. The HPLC method was validated according to ICH Q2(R1) guidelines. Linearity was confirmed over the range of 10–1000 µg/mL (R^2 = 0.9989).

Intra-day and inter-day precision (expressed as RSD%) were <2%. All experiments were conducted in triplicate, and mean values were reported.

2.7. Determination of Encapsulation Efficiency

Encapsulation efficiency (EE%) was calculated as the percentage of encapsulated quercetin relative to the total amount of quercetin initially added to the formulation [31]. Briefly, the nanoparticle suspension was centrifuged at 10,000 rpm for 20 min, and the supernatant was collected. The concentration of unencapsulated quercetin was measured using HPLC under the same chromatographic conditions described above. Encapsulation efficiency was calculated using the formula:

$$EE\% = [(\text{Total Quercetin} - \text{Free Quercetin})/\text{Total Quercetin}] \times 100 \quad (3)$$

All measurements were performed in triplicate, and the results were expressed as mean ± standard deviation.

2.8. Preparation of Chitosan Lactate Nanoparticle-Based Gel

A nanoparticle-loaded hydrogel was formulated using xanthan gum as a gelling agent and Cosgard (a broad-spectrum preservative) to ensure microbiological stability. Briefly, 1% (*w*/*v*) xanthan gum was dispersed in deionized water under continuous stirring at room temperature until a smooth and homogeneous hydrogel base was obtained [32]. In parallel, 10 g of lyophilized chitosan lactate nanoparticles were rehydrated in deionized water at a concentration of 1 mg/mL under continuous magnetic stirring. The nanoparticle suspension was then gradually incorporated into the xanthan gum hydrogel under continuous stirring. Cosgard was added at a final concentration of 0.6% (*v*/*v*), followed by pH adjustment to 6.0–6.5 to ensure the physicochemical stability of the formulation. The resulting bioactive hydrogel was transferred into sterile containers and stored at 4 °C until further analysis.

2.9. Accelerated Stability Assay Assessment

To evaluate the physicochemical stability of the chitosan lactate nanoparticle-based gel, accelerated stability testing was conducted under controlled environmental conditions. Samples of the formulated hydrogel were stored in airtight containers and incubated at 40 ± 2 °C with 75 ± 5% relative humidity in a stability chamber for a period of 60 days, simulating long-term storage conditions [33] in accordance with ICH Q1A(R2) guidelines for semisolid formulations. At predetermined intervals (0, 15, 30, and 30 days), the formulations were assessed for any changes in appearance (color, phase separation, and consistency), pH, and viscosity. Viscosity was measured using a Brookfield DV2T viscometer with spindle LV-64 at 25 °C and 50 rpm. The pH was monitored with a 1/10 (*w*/*w*) dilution in deionised water using a calibrated digital pH meter.

2.10. Microbial Stability Assay Assessment

Microbial stability of the chitosan lactate nanoparticle-based hydrogel was evaluated during the 60-day accelerated stability test. Samples were visually inspected at intervals (0, 15, 30, and 60 days) for turbidity, odor, or visible growth. Additionally, aliquots were cultured on nutrient and Sabouraud dextrose agar to detect bacterial and fungal contamination. Plates were incubated at 37 °C for 48 h (bacteria) and 25 °C for 5 days (fungi). No microbial growth was observed, confirming the antimicrobial preservation efficacy of the Cosgard-containing hydrogel formulation under stress conditions [34].

2.11. Statistical Analysis

Experimental design and statistical analysis were executed employing the NemrodW program (version 2000, LPRAI, Marseille, France). The examination of significant differences among the means of independent variables was carried out through analysis of variance (ANOVA) utilizing IBM SPSS Statistics Software (Version 20.0, IBM SPSS Inc., Armonk, NY, USA), followed by Duncan's multiple range test at a significance level of $p < 0.05$.

3. Results

3.1. Chitosan and Chitosan Lactate Characterization

The FTIR spectral profile of chitosan exhibited characteristic absorption bands associated with polysaccharide biopolymers (Figure 2a). A broad and intense band around 3425 cm^{-1} was attributed to overlapping O–H and N–H stretching vibrations, confirming the presence of hydroxyl and free amino groups. The peak at 2920 cm^{-1} corresponded to aliphatic C–H stretching, while the sharp band at 1655 cm^{-1} was assigned to the amide I band, reflecting residual N-acetyl groups. Bands observed at 1420 and 1320 cm^{-1} were used to estimate the degree of deacetylation (DD), and the absence of a distinct signal around 1730 cm^{-1} further supported the high deacetylation level of the biopolymer, consistent with the titrimetric analysis.

Following lactate modification, notable shifts and new peaks appeared in the FTIR spectrum of chitosan lactate (Figure 2b), indicating successful chemical interaction between chitosan and lactic acid. A slight shift of the broad O–H and N–H stretching band to 3280 cm^{-1} suggests enhanced hydrogen bonding due to lactate incorporation. The appearance of a distinct band at 1729 cm^{-1}, corresponding to C=O stretching of ester or carboxylic groups, confirms the presence of lactate moieties. Moreover, peaks at 1571, 1453, and 1261 cm^{-1}, corresponding to N–H bending, CH bending, and C–N stretching, respectively, reinforce the formation of ionic and covalent interactions. The retention of the strong signal at 1120 cm^{-1}, associated with C–O–C stretching, demonstrates that the polysaccharide backbone remained intact after functionalization.

The comparative characterization of chitosan and its lactate derivative highlights significant modifications in physicochemical properties following lactate complexation (Table 1). The degree of deacetylation (DD) of chitosan, determined by both FTIR (92.33%) and titrimetric (91.53%) methods, confirms its high purity and functional amine availability. These values are consistent with high-grade chitosan suitable for biomedical and pharmaceutical applications. The viscosity of chitosan (52 cP) was reduced upon lactate formation (41 cP), which may be attributed to disruption of intra- and intermolecular hydrogen bonding by lactate ions, leading to increased molecular mobility. Interestingly, chitosan lactate exhibited full dispersion without visible agglomerates in neutral water (pH 7), in contrast to the parent chitosan, which remained insoluble. This improvement in aqueous solubility is particularly advantageous for drug delivery and topical formulations, where physiological pH compatibility is critical. Although the molecular weight of chitosan was estimated at approximately 220 kDa, the corresponding value for chitosan lactate was not determined in this study and warrants further analysis. Both forms presented low ash content (<0.1%), indicative of minimal inorganic contamination. The color shift from off-white (chitosan) to pale yellow (chitosan lactate) may reflect structural changes and the formation of lactate complexes. Overall, the transformation into chitosan lactate enhances functional attributes desirable for advanced bioactive carrier systems.

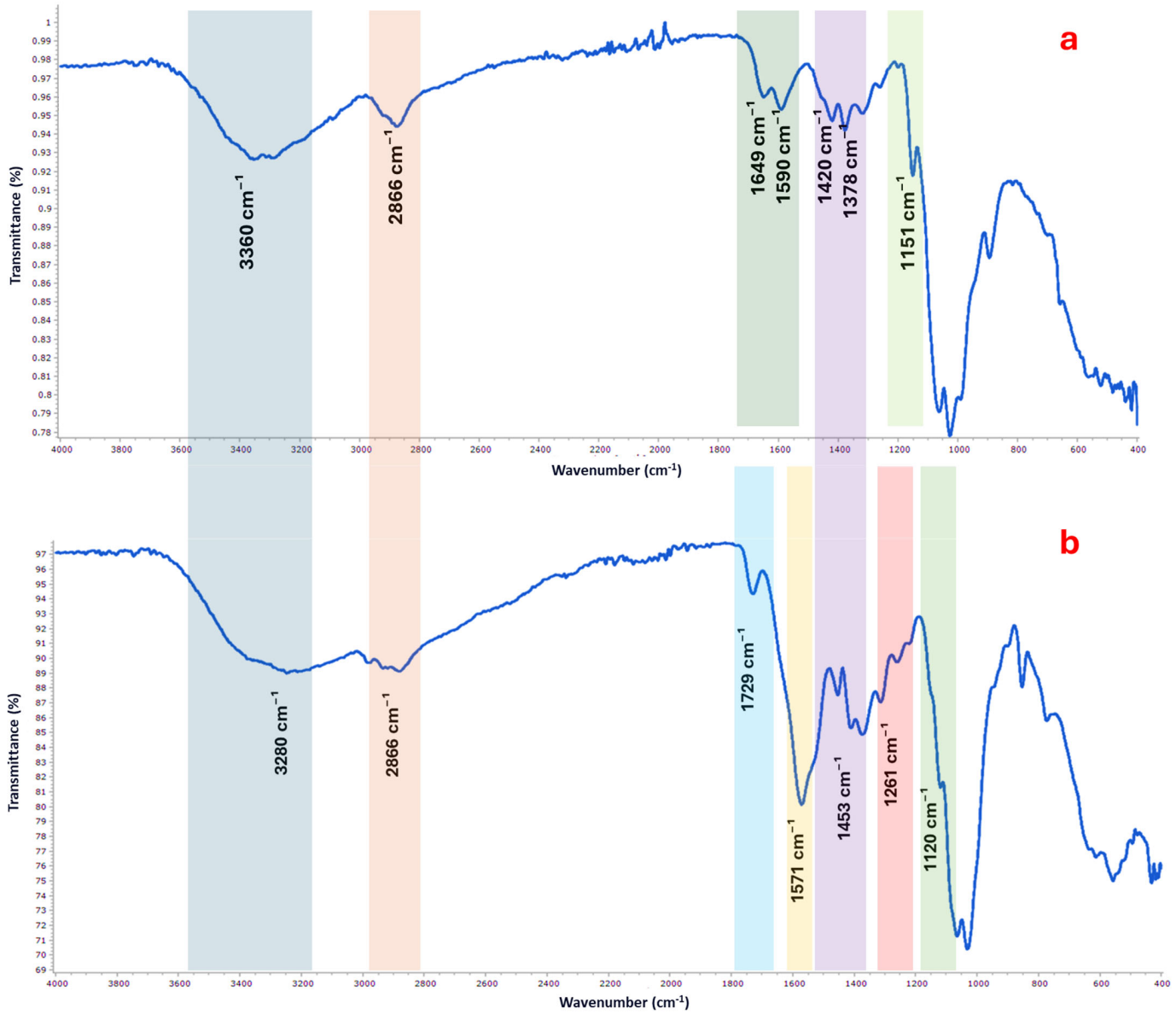

Figure 2. FTIR spectrum of chitosan (**a**) and chitosan lactate (**b**) showing characteristic absorption bands of functional groups.

Table 1. Physicochemical properties of chitosan and chitosan lactate.

Parameter	Chitosan	Chitosan Lactate
Degree of deacetylation (FTIR method)	92.33%	–
Degree of deacetylation (titrimetric method)	91.53%	–
Viscosity in 1% acetic acid (cP)	52	41
Molecular weight	Medium (≈220 kDa)	–
Ash content (%)	0.09%	0.08%
Color	Pale yellow	Pale yellow
Solubility in water (pH 7)	Insoluble	Totally soluble

3.2. Chitosan Lactate Nanoparticle Preparation Using Response Surface Methodology

3.2.1. Experimental Design

In this study, a Box–Behnken experimental design was employed to systematically explore and optimize the formulation parameters affecting the synthesis of chitosan lactate–quercetin nanoparticles. Three independent variables were selected: chitosan concentration (ranging from 1 to 3% *m*/*v*), quercetin concentration (5 to 15 mg/mL), and citric acid concentration (1 to 3% *m*/*v*), which acts as a natural cross-linking agent. The main responses evaluated were nanoparticle size (in nm) and zeta potential (in mV), both of which are critical for ensuring stability, bioavailability, and effective skin delivery in cosmetic applications. A total of 17 experimental runs were performed, including replicates at the central point to assess experimental error and model predictability. The collected data revealed considerable variability in nanoparticle size (from 413.26 to 801.56 nm) and zeta potential (from +22.32 to +39.53 mV), highlighting the significant impact of formulation variables and their interactions. This design allowed for the generation of second-order polynomial models capable of accurately describing the behavior of the system. The experimental matrix and corresponding response values are presented in Table 2. The subsequent statistical analysis was used to identify the most influential factors and to predict the optimal conditions for achieving nanoparticles with desirable physicochemical characteristics suitable for topical hydrogel incorporation.

Table 2. Experimental conditions and responses obtained using the Box-Behnken design.

Exp	Variables Responses				
	Chitosan % *m*/*v*	**Quercitin mg/mL**	**Citric Acid % *m*/*v***	**Size nm**	**Zeta mV**
1	1	5	1	429.69	+29
2	3	5	3	798.69	+39.34
3	1	5	1	476.56	+34.25
4	3	5	3	801.56	+32.34
5	1	10	1	445.31	+30.35
6	3	10	3	756.31	+39.53
7	1	10	1	440.94	+39.5
8	3	10	3	785.94	+35.97
9	2	5	2	450.75	+36.21
10	2	15	2	515.63	+22.32
11	2	5	2	484.38	+29.11
12	2	5	2	473.25	+32.3
13	2	10	2	422.24	+35.33
14	2	10	2	420.51	+32.24
15	2	10	2	424.78	+31.55
16	2	10	2	416.30	+32.86
17	2	10	2	413.26	+30.99

3.2.2. Validity of Models Through ANOVA Analysis

The validity of the second-order polynomial models for predicting nanoparticle size (Y_{size}) and zeta potential (Y_{zeta}) was assessed through analysis of variance (ANOVA), as detailed in Table 3. For the Y_{size} model, the regression analysis revealed a highly significant fit, with an F-test value of 684.496, which exceeded the critical value of F_{tab} = 3.29, indicating that the model significantly explained the variability in nanoparticle size. The R^2 value of 0.994 and adjusted R^2 value of 0.98 further confirmed the robustness of the model, suggesting a strong correlation between the experimental conditions and the observed responses. The significance level of *** ($p < 0.001$) further supports the model's validity. In contrast, for Y_{zeta}, the regression model also demonstrated statistical significance, with an

F-test value of 9.623, which was greater than F_{tab} = 3.29, and an R^2 value of 0.925, with an adjusted R^2 of 0.829. While the model for zeta potential was significant, the validity *p*-value of 36.60% indicated a lower explanatory power compared to Y_{size}. These findings suggest that while both models are statistically valid, the Y_{size} model exhibits a higher degree of fit and predictive accuracy.

Table 3. Analysis of variance (ANOVA) of second-order polynomial models for the two responses.

Source of Variation	Sum of Squares	Degrees of Freedom	Mean Squares	Fisher's F-Test	Significance
Nanoparticle size (Y_{size})					
Regression	363,116	9	40,346.2	684.496	***
Lack of fit	327.019	3	109.006	5.0949	7.6%
R^2 = 0.994		$F_{Obs}(684.496) > F_{tab}(3.29)$			
R_{adj}^2 = 0.98					
Zeta potential (Y_{zeta})					
Regression	287.5618	9	31.9513	9.623	**
Lack of fit	11.8969	3	3.9656	1.398	36.60%
R^2 = 0.925		$F_{Obs}(9.623) > F_{tab}(3.29)$			
R_{adj}^2 = 0.829					

The significance levels are represented as follows: ***: Very significant, **: Significant.

3.2.3. Interpretation of Coefficients

The regression coefficients for the second-order polynomial models predicting nanoparticle size and zeta potential, as presented in Table 4, provide insights into the influence of various terms on the responses. For Y_{size}, the intercept (b_0) coefficient is 419.418 and is highly significant (***), indicating a baseline value for nanoparticle size when all other variables are at their reference levels. The linear effects of the individual variables, chitosan (b_1), quercetin (b_2), and citric acid (b_3), reveal that chitosan concentration (b_1 = 168.75, ***) has the most substantial effect on nanoparticle size, followed by quercetin concentration (b_2 = 12.937, **), while citric acid has a relatively smaller and less significant impact (b_3 = 2.063, 47.70%). The quadratic effects highlight that chitosan concentration (b_{11} = 166.666, ***) and quercetin concentration (b_{22} = 40.541, ***) have significant non-linear effects on nanoparticle size, whereas citric acid (b_{33} = 21.041, ***) also significantly influences size but to a lesser extent. The interaction effects suggest that the combination of chitosan and quercetin (b_{12} = −11, *), as well as quercetin and citric acid (b_{23} = −19, **), significantly influence nanoparticle size, with negative coefficients indicating an antagonistic effect.

For Y_{zeta}, the intercept (b_0) coefficient is 32.594 (***), indicating the baseline zeta potential. The linear effects reveal that quercetin (b_2 = −1.556, *) and citric acid (b_3 = 1.059, 14.20%) have significant and marginally significant effects on zeta potential, with quercetin exerting a negative influence, suggesting it decreases zeta potential, while citric acid has a positive effect. The quadratic effects indicate that chitosan (b_{11} = 3.746, **), quercetin (b_{22} = −2.607, *), and citric acid (b_{33} = −0.002, 99.40%) contribute significantly or marginally to zeta potential changes, with citric acid having an almost negligible quadratic effect. The interaction effects suggest significant influences on zeta potential, with the combination of chitosan and quercetin (b_{12} = −3.063, *), as well as quercetin and citric acid (b_{23} = 4.27, **), playing key roles in determining zeta potential. The response equations with significant coefficients are as follows:

$$Y_{size} = 419.418 + 168.75X_1 + 12.937X_2 + 166.666X_1^2 + 40.541X_2^2 + 21.041X_3^2 - 11X_1X_2 - 19X_2X_3 \quad (4)$$

$$Y_{zeta} = 32.594 + 1.76X_1 - 1.556X_2 + 1.059X_3 + 3.746X_1^2 - 2.607X_2^2 - 3.063X_1X_2 - 3.178X_1X_3 + 4.27X_2X_3 \quad (5)$$

Table 4. Regression coefficients of the second-order polynomial models predicted for the two responses studied.

Termes	Y_{size}		Y_{zeta}	
	Coefficient	**Signification %**	**Coefficient**	**Signification %**
b_0	419.418	***	32.594	***
		Linear Effect		
b_1	168.75	***	1.76	*
b_2	12.937	**	−1.556	*
b_3	2.063	47.70%	1.059	14.20%
		Quadratic Effect		
b_{11}	166.666	***	3.746	**
b_{22}	40.541	***	−2.607	*
b_{33}	21.041	***	−0.002	99.40%
		Interaction Effect		
b_{12}	−11	*	−3.063	*
b_{13}	8.5	6.10%	−3.178	*
b_{23}	−19	**	4.27	**

The significance levels are represented as follows: ***: Very significant, **: Significant, *: Marginally significant.

3.2.4. Analysis of Response Surface Curves

The 3D response surface plots and corresponding 2D contour plots provide valuable insight into the interactive effects of chitosan and quercetin concentrations on nanoparticle size and zeta potential. As illustrated in Figure 3a, nanoparticle size was strongly influenced by both variables, exhibiting a pronounced U-shaped response. At intermediate levels of chitosan (around 2% m/v) and lower quercetin concentrations, the smallest particle sizes (approximately 420–450 nm) were observed. Increasing either chitosan or quercetin concentrations beyond this optimal zone led to a sharp rise in particle size, likely due to excessive polymer matrix or saturation effects that promote nanoparticle aggregation and entanglement. This behavior reflects the strong quadratic and interaction terms observed in the regression model, particularly the significant b_{11} and b_{12} coefficients. The contour plot further confirms the existence of a well-defined minimum region (blue zone), indicating an optimal range of component ratios that yield smaller, more stable nanoparticles. This suggests a balance between sufficient polymer availability to encapsulate quercetin and controlled cross-linking density to prevent oversizing. In contrast, Figure 3b shows that zeta potential increased with rising chitosan concentration, with the highest values (>39 mV) achieved at the upper end of the chitosan range, regardless of quercetin concentration. This trend is consistent with chitosan's cationic nature, as more free amino groups are available to confer positive surface charge. The relatively flatter surface and gradually spaced contour lines imply a less pronounced quadratic effect and a more linear relationship between chitosan content and zeta potential. Notably, the zeta potential remained above 30 mV across much of the design space, indicating good colloidal stability in most formulations. Together, the surface and contour plots support the desirability analysis outcomes and highlight the critical role of polymer-to-drug ratio optimization in tuning nanoparticle properties for enhanced stability and topical performance.

The optimal formulation conditions for chitosan–quercetin–citric acid nanoparticles were determined using the desirability function approach, aiming to minimize particle size while maximizing zeta potential. As summarized in Table 5, the optimal values of the formulation variables were found to be 1.8% (m/v) chitosan, 6.5 mg/mL quercetin, and 1.3% (m/v) citric acid. Under these conditions, the predicted particle size was 399.72 nm and the predicted zeta potential was 30.94 mV. The experimental validation of these predicted responses yielded an observed particle size of 422.02 ± 21.05 nm and a zeta potential of

+29.49 ± 1.22 mV, confirming the accuracy and robustness of the optimization model. The overall desirability score of 99.95% further confirms the effectiveness and precision of the optimization process, validating the suitability of the identified conditions for producing nanoparticles with desirable physicochemical characteristics.

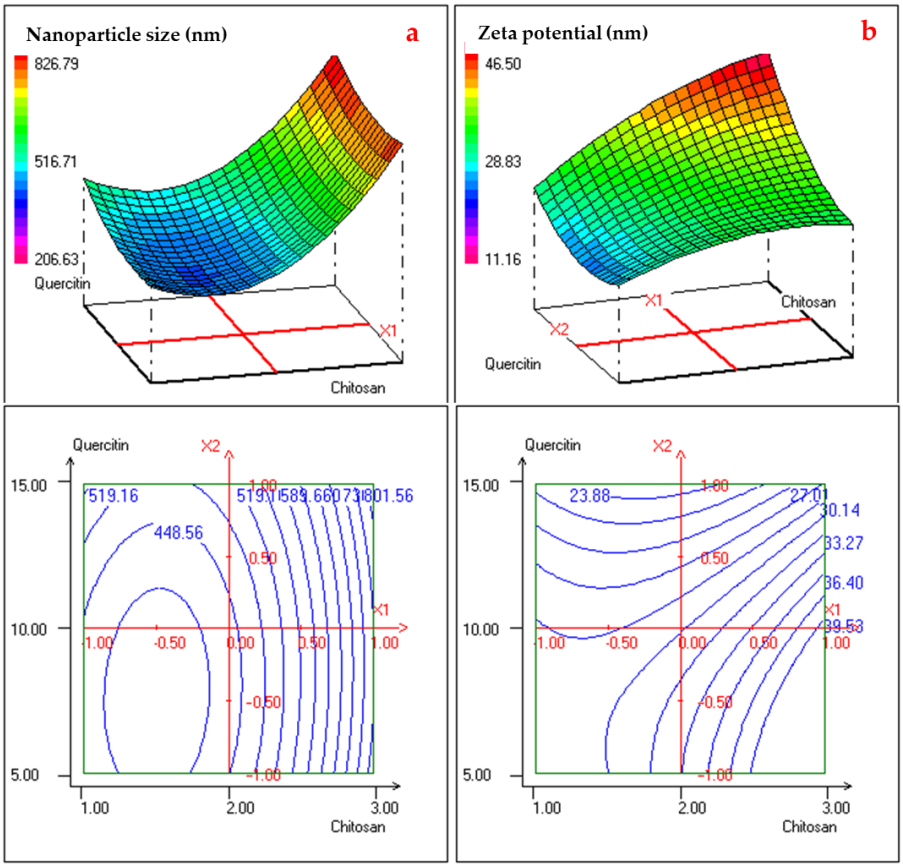

Figure 3. 2D and 3D Response Surface Curves illustrating the effect of the interaction two studied responses: nanoparticle size (**a**) and zeta potential (**b**).

Table 5. Optimal conditions and desirability analysis for nanoparticle formulation.

Factor	Actual Value	Response	Predicted Value	Observed Value
Chitosan (X_1)	1.8% (*m*/*v*)	Particle Size (nm)	399.72	422.02 ± 21.05
Quercetin (X_2)	6.5 mg/mL	Zeta Potential (mV)	+30.94	+29.49 ± 1.22
Citric Acid (X_3)	1.3% % (*m*/*v*)			
			Overall Desirability: 99.95	

3.3. Antioxidant Activity of Nanoparticles and Hydrogel Formulations

The antioxidant profiling of chitosan-based nanoparticles and hydrogel formulations revealed a significantly higher potency in the nanoform. As shown in Table 6, the total antioxidant capacity of the nanoparticle formulation reached 1203.63 ± 60.18 mg GAE/mL, nearly double that of the hydrogel (653.74 ± 32.69 mg GAE/mL), indicating enhanced radical scavenging potential in the nanoparticle suspension. This superior activity was further confirmed by the DPPH assay, where the nanoparticles exhibited a markedly lower IC_{50} value (16.63 ± 0.83 µg/mL) compared to the hydrogel (123.81 ± 6.19 µg/mL), reflecting higher efficiency in neutralizing free radicals. The reducing power assay also supported these findings, with a significantly lower EC_{50} for the nanoparticles (12.23 ± 1.61 µg/mL) than for the hydrogel (256.36 ± 12.82 µg/mL), suggesting stronger electron-donating ca-

pacity. These results highlight the critical role of nanoencapsulation in preserving and enhancing the antioxidant properties of active compounds, likely due to improved stability, dispersion, and bioavailability. The data emphasize the potential of nanoparticulate systems as efficient delivery platforms for antioxidant applications in biomedical and cosmeceutical formulations.

Table 6. Antioxidant activities of chitosan-based nanoparticles and hydrogel formulation.

Antioxidant Parameters	Nanoparticle	Gel
Total Antioxidant Capacity (mg GAE/mL)	1203.63 ^{a} ± 60.18	653.74 ^{b} ± 32.69
DPPH (IC_{50}, µg/mL)	16.63 ^{b} ± 0.83	123.81 ^{a} ± 6.19
Reducing Power (EC_{50}, µg/mL)	12.23 ^{b} ± 1.61	256.36 ^{a} ± 12.82

Results were represented by Means of at least three replicates ± standard deviation, followed by different letters (a, b) show significant differences at $p \leq 0.05$.

3.4. Antibacterial Activity of Chitosan–Quercetin Nanoparticles and Hydrogel Form

The antibacterial efficacy of chitosan–quercetin nanoparticles and their hydrogel formulation was evaluated against five reference bacterial strains by determining the minimum inhibitory concentration (MIC) and minimum bactericidal concentration (MBC), as shown in Figure 4. The nanoparticles exhibited notable antibacterial activity, particularly against *Escherichia coli* ATCC 35218, with both MIC and MBC values of 1.56 and 3.13 µg/mL, respectively, comparable to the standard antibiotic streptomycin. *Pseudomonas aeruginosa* and *Bacillus cereus* were also sensitive to the nanoparticulate formulation (MIC = 3.13 µg/mL; MBC = 3.13 µg/mL), while *Staphylococcus aureus* and *Klebsiella aerogenes* required higher MICs (6.25 µg/mL), indicating a moderate antibacterial effect. In contrast, the hydrogel form demonstrated significantly weaker activity across all strains, with MIC values ranging from 25 to 75 µg/mL, suggesting reduced bioavailability or slower release of the active agents. Overall, the nanoparticle formulation showed a stronger and broader antibacterial spectrum compared to the gel, underscoring its potential as an effective antimicrobial agent.

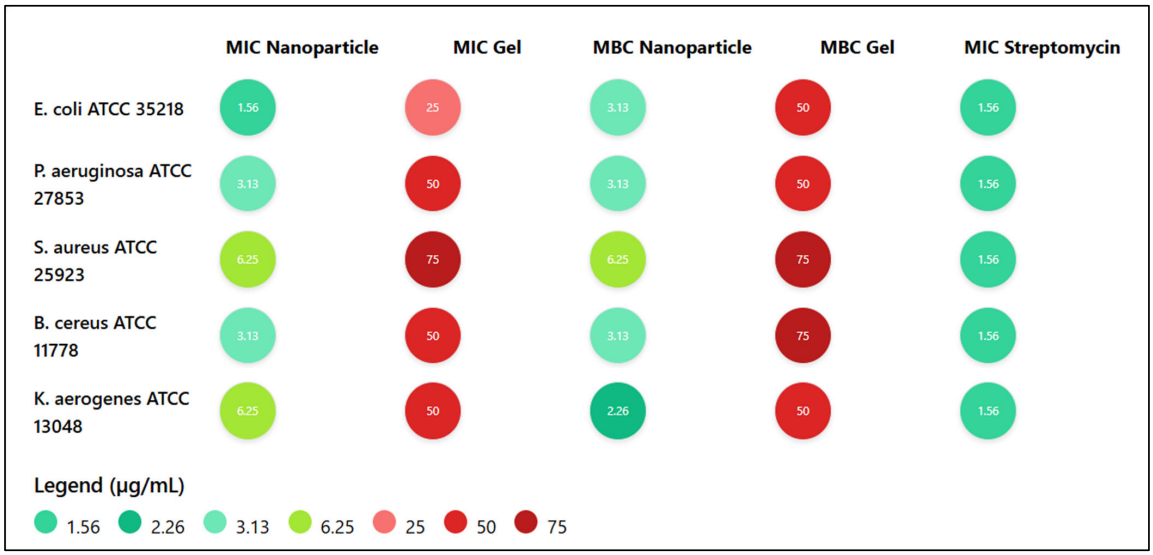

Figure 4. Antibacterial activity of chitosan-quercetin nanoparticles and gel: MIC and MBC values (µg/mL) compared to streptomycin.

3.5. HPLC Analysis of Chitosan-Based Nanoparticles and Hydrogel Formulation

High-performance liquid chromatography (HPLC) was employed to quantify the quercetin content in both chitosan lactate nanoparticles and the final hydrogel formulation, as well as to determine the encapsulation efficiency of the nanoparticles (calculated as the

percentage of encapsulated quercetin relative to the total amount of quercetin initially added to the formulation). The results, summarized in Table 7, indicate that the quercetin content in the nanoparticles was 1.63 ± 0.08 mg per gram of nanoparticle, reflecting effective loading of the active compound. The encapsulation efficiency was calculated to be 76.9 ± 3.2%, demonstrating that a substantial proportion of quercetin was successfully encapsulated within the chitosan lactate matrix. This high EE% suggests strong interactions between quercetin and the chitosan lactate polymer, likely due to ionic and hydrophobic interactions, which enhance the stability and controlled release potential of the nanoparticles. In the hydrogel formulation, the quercetin content was significantly lower, at 0.162 ± 0.01 mg per gram of gel. This reduction is expected, as the nanoparticles were dispersed within the xanthan gum-based hydrogel matrix, resulting in a lower overall concentration of the active compound. The consistent detection of quercetin in both the nanoparticle and hydrogel samples confirms the stability of the active compound throughout the formulation process.

Table 7. HPLC quantification results for quercetin in nanoparticles and hydrogel formulation.

Assay	Values
Quercetin Content in Nanoparticles (mg/g nanoparticle)	1.63 ± 0.08
Encapsulation Efficiency (%)	76.9 ± 3.2%
Quercetin Content in Hydrogel (mg/g gel)	0.162 ± 0.01

3.6. Characterization and Stability of Cosmetic Gel

The chitosan lactate nanoparticle-based hydrogel was characterized for its physicochemical and microbial stability under accelerated storage conditions (40 ± 2 °C, 75 ± 5% relative humidity) over 60 days, as outlined in Sections 2.8 and 2.9. The results, presented in Table 8, demonstrate the formulation's robustness for potential cosmetic applications. At day 0, the hydrogel exhibited a homogeneous, translucent appearance with no phase separation, a pH of 6.51 ± 0.11, and a viscosity of 920.12 ± 15.23 cP, indicating a stable and user-friendly topical formulation. Over the 60-day period, the hydrogel maintained its structural integrity, with only minor changes observed. By day 15, a slight opaqueness developed, but no phase separation occurred, and the pH (6.43 ± 0.16) and viscosity (910.44 ± 18.73 cP) remained statistically unchanged ($p > 0.05$). At day 15, slight opalescence was noted, with a pH of 6.32 ± 0.21 and a viscosity of 890.86 ± 20.11 cP, still within acceptable ranges for topical gels. By day 60, minor thickening was observed, accompanied by a slight pH decrease to 6.20 ± 0.20 and a viscosity of 870.72 ± 25.82 cP, but these changes were not significant ($p > 0.05$) and did not compromise the hydrogel's homogeneity or applicability. Microbial stability was confirmed throughout the study, with no detectable bacterial or fungal growth at any time point, as assessed by culturing on nutrient and Sabouraud dextrose agar.

Table 8. Accelerated stability results of chitosan lactate nanoparticle-based hydrogel (40 °C ± 2 °C, 75% RH ± 5%, over 60 Days).

Time (Days)	Visual Appearance	pH (±SD)	Viscosity (cP ± SD)	Microbial Contamination
0	Homogeneous, translucent, no phase separation	6.51 ± 0.11	920.12 ± 15.23	Not detected
15	Slight opacification, no separation	6.43 ± 0.16	910.44 ± 18.73	Not detected
30	Mild opalescence, stable consistency	6.32 ± 0.21	890.86 ± 20.11	Not detected
60	Slight thickening, no phase separation	6.20 ± 0.20	870.72 ± 25.82	Not detected

Results were represented by means of at least three replicates ± standard deviation.

4. Discussion

In our study, the developed chitosan lactate–based nanoparticles exhibited favorable physicochemical characteristics, including a particle size of 422.02 ± 21.05 nm, a positive zeta potential of +29.49 ± 1.22 mV, and an encapsulation efficiency of 76.9 ± 3.2%. Compared to unmodified chitosan, the lactate derivative showed enhanced water solubility and reduced viscosity, facilitating nanoparticle formation. Antioxidant assays revealed a significantly higher activity for the nanoparticles (IC_{50} = 16.63 ± 0.83 µg/mL; EC_{50} = 12.23 ± 1.61 µg/mL) than for the gel formulation. Similarly, the antibacterial effect of the nanoparticles was more pronounced, with lower MIC values across tested strains compared to the hydrogel. The hydrogel remained physicochemically and microbiologically stable over 60 days under accelerated conditions, indicating good formulation robustness for dermocosmetic applications.

The formulation of a chitosan lactate–quercetin nanoparticle hydrogel addresses key limitations associated with the topical delivery of quercetin, a potent flavonoid with well-documented antioxidant, anti-inflammatory, and anti-aging properties [6,7]. Despite its therapeutic potential, quercetin suffers from poor water solubility and chemical instability, which significantly limit its incorporation into conventional cosmetic formulations [8]. In this context, the chemical conversion of chitosan into its lactate salt form proved to be a strategic choice.

Chitosan lactate has gained significant attention in the cosmetics industry due to its multifunctional properties, particularly its antimicrobial activity and skin conditioning capabilities [35]. These characteristics make chitosan lactate an attractive ingredient in modern cosmetic formulations, particularly in skin and hair care products. Among its key properties, chitosan lactate exhibits potent antimicrobial activity, contributing to the preservation of formulations and the maintenance of skin health [36]. Additionally, chitosan functions as a natural moisturizing agent, improving skin hydration and texture [37]. Its ability to form a thin, protective film on the skin further aids in moisture retention and shields the skin from environmental aggressors [38]. Chitosan lactate is widely applied across various cosmetic products. In skin care, it is included in serums and creams, often in synergy with ingredients like lactic acid to boost efficacy [35,39]. In hair care formulations, it contributes to improved hair manageability and shine due to its film-forming and hair-fixing properties [35].

The lactate modification significantly improved solubility at physiological pH, making it more suitable for dermal applications, while preserving the essential bioactivity of the polymer [40]. FTIR spectral analysis confirmed the successful interaction between chitosan and lactic acid, with characteristic shifts indicating ionic and hydrogen bonding. These structural modifications, consistent with previous reports [4,41], enhanced molecular flexibility and reduced intra- and intermolecular hydrogen bonding, thus favoring nanoparticle formation. The FTIR spectrum of chitosan is characterized by distinct bands reflecting its functional groups and interactions. Notably, a prominent band around 1647 cm^{-1} corresponds to C=O stretching, while bands near 1550 cm^{-1} are attributed to N-H bending vibrations, indicating the presence of amine groups [42]. Hydroxyl groups contribute to additional bands associated with hydrogen bonding, which influence the solubility and mechanical properties of the material [43]. In chitosan lactate, the introduction of lactic acid alters the FTIR profile by modifying hydrogen bonding patterns and introducing new functional groups, potentially shifting the carbonyl band. This interaction also induces structural changes, resulting in a more amorphous form compared to the partially crystalline nature of native chitosan, thereby affecting its physical properties [44].

In addition, the optimization of nanoparticle formulation using response surface methodology by ionic gelation provided critical insights into the role of each component.

Chitosan concentration exhibited the most pronounced influence on both particle size and zeta potential, a finding in agreement with Pathak et al. [45], where increased polymer content was associated with denser particle matrices and enhanced surface charge. Quercetin contributed non-linearly to both responses, possibly due to its involvement in hydrogen bonding and hydrophobic interactions within the nanoparticle network [46,47]. Citric acid, used as a crosslinker, played a supportive role in stabilizing the particles through ionic bridging without compromising biocompatibility [48]. The generated quadratic models showed strong statistical significance, especially for particle size (R^2 = 0.994), highlighting the robustness of the optimization process. The surface and contour plots provided visual confirmation of these interactions. A distinct minimum region in the response surface for particle size indicated an optimal balance between chitosan and quercetin concentrations, where particles around 420 nm could be obtained. Beyond this region, particle size increased rapidly, likely due to excessive matrix entanglement and polymer–polyphenol saturation effects. Zeta potential increased steadily with chitosan concentration, reflecting the cationic nature of the polymer and supporting electrostatic stabilization, consistent with findings from Németh et al. [49]. These results validate the rationale behind selecting chitosan as a multifunctional carrier in cosmetic nanocarriers.

HPLC analysis confirmed efficient quercetin encapsulation within nanoparticles, with significant loading compared to the gel formulation. Quercetin's polyphenolic structure, featuring multiple hydroxyl and aromatic moieties, enables strong hydrogen bonding and hydrophobic interactions with chitosan lactate's acetylated glucosamine units, ensuring high encapsulation efficiency. This is consistent with Liu et al. [50], who noted that chitosan's polar and non-polar domains stabilize polyphenols through multifaceted interactions [50]. The lower quercetin content in the gel reflects its dispersion within the xanthan gum matrix, where polysaccharide–polyphenol hydrogen bonding may further shield the active compound. Compared to Zhou et al. [51], who reported quercetin degradation in aqueous systems due to oxidative cleavage of its catechol groups, the nanoparticles' protective matrix likely minimizes such reactions, enhancing chemical stability [51].

The nanoparticles exhibited superior antioxidant activity compared to the gel, attributed to enhanced quercetin solubility and protection from oxidative degradation. Chemically, quercetin's 3,5,7,3′,4′-pentahydroxyflavone structure donates electrons to neutralize free radicals, a process amplified by nanoencapsulation's high surface area and stable dispersion. This outperforms gel-based systems, where xanthan gum's viscous network may limit quercetin's accessibility to radicals, as observed by Jadav et al. [52] in polysaccharide-based hydrogels. Compared to Casanova and Santos [53], who reported moderate antioxidant activity in macroscale polyphenol formulations, the nanoparticles' enhanced efficacy underscores the chemical advantage of nanoscale delivery.

Antibacterial activity was notably stronger in nanoparticles, particularly against Gram-negative bacteria, due to synergistic chemical mechanisms. Chitosan lactate's protonated amino groups electrostatically bind to bacterial lipopolysaccharides, disrupting membrane integrity, while quercetin's phenolic groups may chelate metal ions critical for bacterial enzymes. This dual action surpasses the efficacy of chitosan alone, as reported by Imam et al. [54], who noted enhanced antimicrobial effects with polyphenol-loaded chitosan nanoparticles. The hydrogel's reduced activity likely results from hindered diffusion through the xanthan gum matrix, a limitation also observed in hydrogel-encapsulated antimicrobials. Compared to Casadidio et al. [55], who highlighted chitosan's role in preventing cosmetic contamination, the nanoparticles offer superior protection against pathogens like *Pseudomonas aeruginosa*.

Recent studies demonstrate that chitosan–quercetin nanoparticles interact directly with skin cells to enhance antioxidant effects by improving quercetin's solubility, stability,

and cellular uptake. These nanoparticles enable the targeted delivery of quercetin into deeper layers of the skin, thereby enhancing protection against oxidative stress and UV-induced damage [56,57]. The encapsulation of quercetin addresses its major limitations, such as low hydrophilicity and poor percutaneous absorption, making it significantly more effective in topical cosmetic formulations. Notably, zein/chitosan nanoparticles have been shown to increase the solubility of quercetin by 753.6-fold in water, while also protecting it from degradation caused by UV irradiation and heat, thus preserving its antioxidant potential [56]. This encapsulation strategy also improves cellular uptake, restoring the activity of antioxidant enzymes and reducing oxidative stress markers like malondialdehyde (MDA) *in vitro* [56]. Moreover, enhanced percutaneous absorption allows the active compound to penetrate the epidermis more efficiently and interact with skin cells [57]. Mechanistically, quercetin-loaded chitosan nanoparticles inhibit the NF-κB/COX-2 signaling pathway, which plays a key role in inflammation and skin damage, thereby reducing UVB-induced skin edema [57]. The antioxidant potential of these nanoparticles has also been confirmed through various biochemical assays, supporting their value in skincare applications [58]. Nevertheless, while the therapeutic promise is substantial, further research is required to standardize these formulations, assess their long-term dermal safety, and fully evaluate potential toxicity, especially for non-oral applications [46].

Additionally, incorporating chitosan–quercetin nanoparticles into cosmetic formulations presents multiple advantages for skin care, primarily due to their enhanced delivery efficiency and therapeutic potential. The nano-formulation of quercetin improved its aqueous stability and preserved its biological activity *in vitro*, which may support its topical application. These nanoparticles facilitate improved skin penetration by traversing the stratum corneum and ensuring prolonged contact through their mucoadhesive properties, thereby enhancing quercetin's therapeutic impact [59,60]. Encapsulation addresses quercetin's poor solubility and instability, enabling sustained release and improved efficacy in treating skin conditions compared to its free form [61]. Beyond acting as a delivery vehicle, chitosan also contributes moisturizing and conditioning effects, making it valuable in both skin and hair care formulations [35]. The synergistic action of quercetin's antioxidant and anti-inflammatory properties with chitosan's skin-conditioning benefits supports the development of multifunctional cosmetic products [61]. Nevertheless, despite these promising attributes, further research is essential to understand long-term effects and optimize formulations, as the standardization and scalability of chitosan-based systems remain significant challenges for their broader adoption in cosmetic applications [62].

Despite the relatively low concentration of quercetin incorporated into the formulation, the *in vitro* assays revealed significant antioxidant and antimicrobial effects. This outcome can be attributed to the high intrinsic bioactivity of quercetin, which has been shown to remain effective at micromolar concentrations [63]. Moreover, encapsulation within chitosan lactate nanoparticles enhances local bioavailability, improves aqueous dispersion, and protects quercetin from oxidative degradation, thereby increasing its functional stability and efficacy. To further support this point, we compared quercetin with rutin, a structurally related glycosylated flavonoid. Although rutin is more hydrophilic, its antioxidant activity is often lower than that of quercetin due to steric hindrance from its sugar moiety, which limits radical scavenging efficiency [64,65]. Therefore, the observed biological activity of our formulation can be reasonably explained by the superior potency of quercetin, even at reduced concentrations.

The hydrogel's stability under accelerated conditions, with minimal changes in pH, viscosity, or appearance, reflects the chemical stability of the xanthan gum–chitosan lactate system. Xanthan gum's anionic galacturonate residues form a robust network that stabilizes nanoparticles, preventing aggregation, while Cosgard's paraben-free preservatives inhibit

microbial enzyme activity. These results align with Alves et al. [66], who reported stable polysaccharide gels under thermal stress. In contrast to certain chitosan hydrogels that undergo phase separation due to polymer hydrolysis, the hydrogel's stability indicates robust intermolecular interactions, likely strengthened by citric acid-mediated crosslinking [67].

The present study offers a comprehensive formulation and optimization of a quercetin-loaded chitosan lactate nanoparticle hydrogel, highlighting its antioxidant and antibacterial efficacy for potential dermocosmetic use. A key strength lies in the use of chitosan lactate, which enhanced aqueous solubility and facilitated nanoparticle formation under mild, green conditions. The application of response surface methodology allowed precise optimization of formulation variables, and the physicochemical stability of the hydrogel under accelerated conditions supports its practical relevance. However, certain limitations should be acknowledged. First, the *in vitro* tests did not include a free quercetin control, limiting direct comparisons of nanoparticle-mediated efficacy. Second, the stability assay was only conducted under accelerated conditions, without parallel testing at room or refrigerated temperatures. Another limitation of this study is the lack of release profile characterization for quercetin from both nanoparticles and hydrogel. The kinetic behavior of drug release is critical to understand the sustained activity and bioavailability, especially for topical applications. This will be explored in future work using appropriate *in vitro* diffusion models. Finally, although the study demonstrated promising *in vitro* bioactivity, *in vivo* validation and skin permeation assays are necessary to fully assess the formulation's dermal applicability.

5. Conclusions

This study successfully demonstrates the development of a multifunctional hydrogel based on chitosan lactate–quercetin nanoparticles with potent antioxidant and antibacterial activities for topical cosmetic applications. The chemical modification of chitosan into its lactate form enhanced its solubility and suitability for nanoparticle formation at physiological pH. Optimization via response surface methodology led to a stable nanoformulation with desirable physicochemical properties, high quercetin encapsulation efficiency, and strong *in vitro* antioxidant and antibacterial activity. When incorporated into a xanthan gum hydrogel, the system maintained its structural and microbiological stability under accelerated conditions for 60 days. The superior performance of the nanoparticle formulation, compared to the base gel, underscores the potential of this natural, bioactive, and eco-friendly platform for next-generation dermocosmetic products targeting oxidative stress and skin-associated pathogens. Future studies should explore *in vivo* skin permeation, long-term safety, and consumer acceptability to support clinical translation and commercial development.

Author Contributions: Conceptualization, R.Y., M.H. and M.S.T.; methodology, R.Y., M.H., H.G., A.B.A., S.S., K.Z., K.H.-N., I.B.R. and M.S.T.; software, R.Y., M.H. and H.G.; validation, M.H., K.H.-N., I.B.R. and M.S.T.; formal analysis, R.Y., M.H., H.G. and K.Z.; investigation, R.Y., M.H., K.Z., I.B.R. and M.S.T.; resources, R.Y., M.H., K.H.-N. and M.S.T.; data curation, R.Y., M.H., H.G., I.B.R. and M.S.T.; writing—original draft preparation, R.Y. and M.H.; writing—review and editing, R.Y., M.H., I.B.R. and M.S.T.; visualization, R.Y., M.H., H.G., I.B.R. and M.S.T.; supervision, M.S.T.; project administration, M.S.T.; funding acquisition, I.B.R. and M.S.T. All authors have read and agreed to the published version of the manuscript.

Funding: This research was funded by the CHITPHAN project (Funding code: Collabora-Technopôle-16), a collaborative project between LPAM/CBBC, LPCMMA/CNRSM, and Startup CHITELIX, under the Tunisian Programme of Collaborative Research-Innovation Projects within Technoparks.

Institutional Review Board Statement: Not applicable.

Informed Consent Statement: Not applicable.

Data Availability Statement: The data presented in this study are available on request from the corresponding author.

Conflicts of Interest: The authors declare no conflicts of interest.

References

1. Kim, M.; Shin, M.; Zhao, Y.; Ghosh, M.; Son, Y.-O. Transformative Impact of Nanocarrier-Mediated Drug Delivery: Overcoming Biological Barriers and Expanding Therapeutic Horizons. *Small Sci.* **2024**, *4*, 2400280. [CrossRef] [PubMed]
2. Detsi, A.; Kavetsou, E.; Kostopoulou, I.; Pitterou, I.; Pontillo, A.R.N.; Tzani, A.; Christodoulou, P.; Siliachli, A.; Zoumpoulakis, P. Nanosystems for the Encapsulation of Natural Products: The Case of Chitosan Biopolymer as a Matrix. *Pharmaceutics* **2020**, *12*, 669. [CrossRef] [PubMed]
3. Yadav, M.; Kaushik, B.; Rao, G.K.; Srivastava, C.M.; Vaya, D. Advances and Challenges in the Use of Chitosan and Its Derivatives in Biomedical Fields: A Review. *Carbohydr. Polym. Technol. Appl.* **2023**, *5*, 100323. [CrossRef]
4. Weecharangsan, W.; Opanasopit, P.; Ngawhirunpat, T.; Rojanarata, T.; Apirakaramwong, A. Chitosan Lactate as a Nonviral Gene Delivery Vector in COS-1 Cells. *AAPS PharmSciTech* **2017**, *7*, 66. [CrossRef]
5. Pieklarz, K.; Galita, G.; Tylman, M.; Maniukiewicz, W.; Kucharska, E.; Majsterek, I.; Modrzejewska, Z. Physico-Chemical Properties and Biocompatibility of Thermosensitive Chitosan Lactate and Chitosan Chloride Hydrogels Developed for Tissue Engineering Application. *J. Funct. Biomater.* **2021**, *12*, 37. [CrossRef]
6. Batiha, G.E.-S.; Beshbishy, A.M.; Ikram, M.; Mulla, Z.S.; El-Hack, M.E.A.; Taha, A.E.; Algammal, A.M.; Elewa, Y.H.A. The Pharmacological Activity, Biochemical Properties, and Pharmacokinetics of the Major Natural Polyphenolic Flavonoid: Quercetin. *Foods* **2020**, *9*, 374. [CrossRef]
7. Vollmannová, A.; Bojňanská, T.; Musilová, J.; Lidiková, J.; Cifrová, M. Quercetin as One of the Most Abundant Represented Biological Valuable Plant Components with Remarkable Chemoprotective Effects—A Review. *Heliyon* **2024**, *10*, e33342. [CrossRef]
8. Wang, W.; Sun, C.; Mao, L.; Ma, P.; Liu, F.; Yang, J.; Gao, Y. The Biological Activities, Chemical Stability, Metabolism and Delivery Systems of Quercetin: A Review. *Trends Food Sci. Technol.* **2016**, *56*, 21–38. [CrossRef]
9. Nishimoto-Sauceda, D.; Romero-Robles, L.E.; Antunes-Ricardo, M. Biopolymer Nanoparticles: A Strategy to Enhance Stability, Bioavailability, and Biological Effects of Phenolic Compounds as Functional Ingredients. *J. Sci. Food Agric.* **2022**, *102*, 41–52. [CrossRef] [PubMed]
10. Ghasemiyeh, P.; Mohammadi-Samani, S. Potential of Nanoparticles as Permeation Enhancers and Targeted Delivery Options for Skin: Advantages and Disadvantages. *Drug Des. Dev. Ther.* **2020**, *14*, 3271–3289. [CrossRef]
11. Ammala, A. Biodegradable Polymers as Encapsulation Materials for Cosmetics and Personal Care Markets. *Int. J. Cosmet. Sci.* **2013**, *35*, 113–124. [CrossRef] [PubMed]
12. Szulc-Musioł, B.; Sarecka-Hujar, B. The Use of Micro- and Nanocarriers for Resveratrol Delivery into and across the Skin in Different Skin Diseases—A Literature Review. *Pharmaceutics* **2021**, *13*, 451. [CrossRef] [PubMed]
13. Ferreira, P.G.; Ferreira, V.F.; da Silva, F.d.C.; Freitas, C.S.; Pereira, P.R.; Paschoalin, V.M.F. Chitosans and Nanochitosans: Recent Advances in Skin Protection, Regeneration, and Repair. *Pharmaceutics* **2022**, *14*, 1307. [CrossRef]
14. Elnagar, M.A.; Khalil, R.H.; Talaat, T.S.; Sherif, A.H. A Blend of Chitosan-Vitamin C and Vitamin E Nanoparticles Robust the Immunosuppressed-Status in Nile Tilapia Treated with Salt. *BMC Vet. Res.* **2024**, *20*, 331. [CrossRef]
15. Patel, J.; Maji, B.; Narayana Moorthy, N.S.H.; Maiti, S. Xanthan Gum Derivatives: Review of Synthesis, Properties and Diverse Applications. *RSC Adv.* **2020**, *10*, 27103–27136. [CrossRef]
16. Raghavendra Naveen, N.; Kurakula, M.; Gowthami, B. Process Optimization by Response Surface Methodology for Preparation and Evaluation of Methotrexate Loaded Chitosan Nanoparticles. *Mater. Today Proc.* **2020**, *33*, 2716–2724. [CrossRef]
17. Pochapski, D.J.; Carvalho dos Santos, C.; Leite, G.W.; Pulcinelli, S.H.; Santilli, C.V. Zeta Potential and Colloidal Stability Predictions for Inorganic Nanoparticle Dispersions: Effects of Experimental Conditions and Electrokinetic Models on the Interpretation of Results. *Langmuir* **2021**, *37*, 13379–13389. [CrossRef] [PubMed]
18. Neza, E.; Centini, M. Microbiologically Contaminated and Over-Preserved Cosmetic Products According Rapex 2008–2014. *Cosmetics* **2016**, *3*, 3. [CrossRef]
19. Baxter, A.; Dillon, M.; Anthony Taylor, K.D.; Roberts, G.A.F. Improved Method for i.r. Determination of the Degree of *N*-Acetylation of Chitosan. *Int. J. Biol. Macromol.* **1992**, *14*, 166–169. [CrossRef]
20. Tolaimate, A.; Desbrières, J.; Rhazi, M.; Alagui, A.; Vincendon, M.; Vottero, P. On the Influence of Deacetylation Process on the Physicochemical Characteristics of Chitosan from Squid Chitin. *Polymer* **2000**, *41*, 2463–2469. [CrossRef]
21. Baxter, S.; Zivanovic, S.; Weiss, J. Molecular Weight and Degree of Acetylation of High-Intensity Ultrasonicated Chitosan. *Food Hydrocoll.* **2005**, *19*, 821–830. [CrossRef]

22. Czechowska-Biskup, R.; Wach, R.A.; Rosiak, J.M.; Ulański, P. Procedure for Determination of the Molecular Weight of Chitosan by Viscometry. *Prog. Chem. Appl. Chitin Its Deriv.* **2018**, *23*, 45–54. [CrossRef]
23. Prieto, P.; Pineda, M.; Aguilar, M. Spectrophotometric Quantitation of Antioxidant Capacity through the Formation of a Phosphomolybdenum Complex: Specific Application to the Determination of Vitamin E. *Anal. Biochem.* **1999**, *269*, 337–341. [CrossRef] [PubMed]
24. Rguez, S.; Papetti, A.; Bourguou, S.; Msaada, K.; Hammami, M.; Mkadmini Hammi, K.; Hamrouni Sellami, I. Antifungal and Antioxidant Effects of Phenolic Acids and Flavonol Glycosides from *Tetraclinis articulata*. *Arch. Phytopathol. Plant Prot.* **2022**, *55*, 284–302. [CrossRef]
25. Yeddes, W.; Chalghoum, A.; Aidi-Wannes, W.; Ksouri, R.; Saidani Tounsi, M. Effect of Bioclimatic Area and Season on Phenolics and Antioxidant Activities of Rosemary (*Rosmarinus officinalis* L.) Leaves. *J. Essent. Oil Res.* **2019**, *31*, 432–443. [CrossRef]
26. Duarte, A.; Ferreira, S.; Silva, F.; Domingues, F.C. Synergistic Activity of Coriander Oil and Conventional Antibiotics against *Acinetobacter baumannii*. *Phytomedicine* **2012**, *19*, 236–238. [CrossRef]
27. Luís, Â.; Duarte, A.; Gominho, J.; Domingues, F.; Duarte, A.P. Chemical Composition, Antioxidant, Antibacterial and Anti-Quorum Sensing Activities of *Eucalyptus globulus* and *Eucalyptus radiata* Essential Oils. *Ind. Crops Prod.* **2016**, *79*, 274–282. [CrossRef]
28. Gutiérrez-Ruíz, S.C.; Cortes, H.; González-Torres, M.; Almarhoon, Z.M.; Gürer, E.S.; Sharifi-Rad, J.; Leyva-Gómez, G. Optimize the Parameters for the Synthesis by the Ionic Gelation Technique, Purification, and Freeze-Drying of Chitosan-Sodium Tripolyphosphate Nanoparticles for Biomedical Purposes. *J. Biol. Eng.* **2024**, *18*, 12. [CrossRef]
29. Vozza, G.; Danish, M.; Byrne, H.J.; Frías, J.M.; Ryan, S.M. Application of Box-Behnken Experimental Design for the Formulation and Optimisation of Selenomethionine-Loaded Chitosan Nanoparticles Coated with Zein for Oral Delivery. *Int. J. Pharm.* **2018**, *551*, 257–269. [CrossRef]
30. Zou, Y.; Qian, Y.; Rong, X.; Cao, K.; McClements, D.J.; Hu, K. Encapsulation of Quercetin in Biopolymer-Coated Zein Nanoparticles: Formation, Stability, Antioxidant Capacity, and Bioaccessibility. *Food Hydrocoll.* **2021**, *120*, 106980. [CrossRef]
31. Valencia, M.S.; Franco da Silva Júnior, M.; Xavier Júnior, F.H.; de Oliveira Veras, B.; Fernanda de Oliveira Borba, E.; Gonçalves da Silva, T.; Xavier, V.L.; Pessoa de Souza, M.; Carneiro-da-Cunha, M.d.G. Bioactivity and Cytotoxicity of Quercetin-Loaded, Lecithin-Chitosan Nanoparticles. *Biocatal. Agric. Biotechnol.* **2021**, *31*, 101879. [CrossRef]
32. Izawa, H.; Kadokawa, J. Preparation and Characterizations of Functional Ionic Liquid-Gel and Hydrogel Materials of Xanthan Gum. *J. Mater. Chem.* **2010**, *20*, 5235–5241. [CrossRef]
33. Larrea-Wachtendorff, D.; Del Grosso, V.; Ferrari, G. Evaluation of the Physical Stability of Starch-Based Hydrogels Produced by High-Pressure Processing (HPP). *Gels* **2022**, *8*, 152. [CrossRef]
34. Schettino, R.; Pontonio, E.; Gobbetti, M.; Rizzello, C.G. Extension of the Shelf-Life of Fresh Pasta Using Chickpea Flour Fermented with Selected Lactic Acid Bacteria. *Microorganisms* **2020**, *8*, 1322. [CrossRef]
35. Guzmán, E.; Ortega, F.; Rubio, R.G. Chitosan: A Promising Multifunctional Cosmetic Ingredient for Skin and Hair Care. *Cosmetics* **2022**, *9*, 99. [CrossRef]
36. Savard, T.; Beaulieu, C.; Boucher, I.; Champagne, C.P. Antimicrobial Action of Hydrolyzed Chitosan against Spoilage Yeasts and Lactic Acid Bacteria of Fermented Vegetables. *J. Food Prot.* **2002**, *65*, 828–833. [CrossRef]
37. Alkabli, J. Recent Advances in the Development of Chitosan/Hyaluronic Acid-Based Hybrid Materials for Skin Protection, Regeneration, and Healing: A Review. *Int. J. Biol. Macromol.* **2024**, *279*, 135357. [CrossRef]
38. Kowalczyk, D.; Karaś, M.; Kordowska-Wiater, M.; Skrzypek, T.; Kazimierczak, W. Inherently Acidic Films Based on Chitosan Lactate-Doped Starches and Pullulan as Carries of Nisin: A Comparative Study of Controlled-Release and Antimicrobial Properties. *Food Chem.* **2023**, *404*, 134760. [CrossRef]
39. Sionkowska, A.; Lewandowska, K.; Kurzawa, M. Chitosan-Based Films Containing Rutin for Potential Cosmetic Applications. *Polymers* **2023**, *15*, 3224. [CrossRef]
40. Lukić, M.; Pantelić, I.; Savić, S.D. Towards Optimal pH of the Skin and Topical Formulations: From the Current State of the Art to Tailored Products. *Cosmetics* **2021**, *8*, 69. [CrossRef]
41. Meyer-Déru, L.; David, G.; Auvergne, R. Chitosan Chemistry Review for Living Organisms Encapsulation. *Carbohydr. Polym.* **2022**, *295*, 119877. [CrossRef]
42. Dimzon, I.K.D.; Knepper, T.P. Degree of Deacetylation of Chitosan by Infrared Spectroscopy and Partial Least Squares. *Int. J. Biol. Macromol.* **2015**, *72*, 939–945. [CrossRef]
43. Qiao, C.; Ma, X.; Wang, X.; Liu, L. Structure and Properties of Chitosan Films: Effect of the Type of Solvent Acid. *LWT* **2021**, *135*, 109984. [CrossRef]
44. Cheng, T.; Hund, R.-D.; Aibibu, D.; Horakova, J.; Cherif, C. Pure Chitosan and Chitsoan/Chitosan Lactate Blended Nanofibres Made by Single Step Electrospinning. *Autex Res. J.* **2013**, *13*, 128–133. [CrossRef]
45. Pathak, R.; Bhatt, S.; Punetha, V.D.; Punetha, M. Chitosan Nanoparticles and Based Composites as a Biocompatible Vehicle for Drug Delivery: A Review. *Int. J. Biol. Macromol.* **2023**, *253*, 127369. [CrossRef]

46. Lawson, M.K. Improvement of Therapeutic Value of Quercetin with Chitosan Nanoparticle Delivery Systems and Potential Applications. *Int. J. Mol. Sci.* **2023**, *24*, 3293. [CrossRef]
47. Zhang, Y.; Hou, R.; Zhu, B.; Yin, G.; Zhang, J.; Zhao, W.; Zhang, J.; Li, T.; Zhang, Z.; Wang, H.; et al. Changes on the Conformational and Functional Properties of Soybean Protein Isolate Induced by Quercetin. *Front. Nutr.* **2022**, *9*, 966750. [CrossRef]
48. Simões, B.M.; Cagnin, C.; Yamashita, F.; Olivato, J.B.; Garcia, P.S.; de Oliveira, S.M.; Eiras Grossmann, M.V. Citric Acid as Crosslinking Agent in Starch/Xanthan Gum Hydrogels Produced by Extrusion and Thermopressing. *LWT* **2020**, *125*, 108950. [CrossRef]
49. Németh, Z.; Csóka, I.; Semnani Jazani, R.; Sipos, B.; Haspel, H.; Kozma, G.; Kónya, Z.; Dobó, D.G. Quality by Design-Driven Zeta Potential Optimisation Study of Liposomes with Charge Imparting Membrane Additives. *Pharmaceutics* **2022**, *14*, 1798. [CrossRef]
50. Liu, J.; Yu, H.; Kong, J.; Ge, X.; Sun, Y.; Mao, M.; Wang, D.Y.; Wang, Y. Preparation, Characterization, Stability, and Controlled Release of Chitosan-Coated Zein/Shellac Nanoparticles for the Delivery of Quercetin. *Food Chem.* **2024**, *444*, 138634. [CrossRef]
51. Zhou, A.; Kikandi, S.; Sadik, O.A. Electrochemical Degradation of Quercetin: Isolation and Structural Elucidation of the Degradation Products. *Electrochem. Commun.* **2007**, *9*, 2246–2255. [CrossRef]
52. Jadav, M.; Pooja, D.; Adams, D.J.; Kulhari, H. Advances in Xanthan Gum-Based Systems for the Delivery of Therapeutic Agents. *Pharmaceutics* **2023**, *15*, 402. [CrossRef]
53. Casanova, F.; Santos, L. Encapsulation of Cosmetic Active Ingredients for Topical Application—A Review. *J. Microencapsul.* **2016**, *33*, 1–17. [CrossRef]
54. Imam, S.S.; Alshehri, S.; Ghoneim, M.M.; Zafar, A.; Alsaidan, O.A.; Alruwaili, N.K.; Gilani, S.J.; Rizwanullah, M. Recent Advancement in Chitosan-Based Nanoparticles for Improved Oral Bioavailability and Bioactivity of Phytochemicals: Challenges and Perspectives. *Polymers* **2021**, *13*, 4036. [CrossRef]
55. Casadidio, C.; Peregrina, D.V.; Gigliobianco, M.R.; Deng, S.; Censi, R.; Di Martino, P. Chitin and Chitosans: Characteristics, Eco-Friendly Processes, and Applications in Cosmetic Science. *Mar. Drugs* **2019**, *17*, 369. [CrossRef]
56. Ma, J.-J.; Yu, Y.-G.; Yin, S.-W.; Tang, C.-H.; Yang, X.-Q. Cellular Uptake and Intracellular Antioxidant Activity of Zein/Chitosan Nanoparticles Incorporated with Quercetin. *J. Agric. Food Chem.* **2018**, *66*, 12783–12793. [CrossRef]
57. Nan, W.; Ding, L.; Chen, H.; Khan, F.U.; Yu, L.; Sui, X.; Shi, X. Topical Use of Quercetin-Loaded Chitosan Nanoparticles Against Ultraviolet B Radiation. *Front. Pharmacol.* **2018**, *9*, 826. [CrossRef]
58. Zhang, Y.; Yang, Y.; Tang, K.; Hu, X.; Zou, G. Physicochemical Characterization and Antioxidant Activity of Quercetin-Loaded Chitosan Nanoparticles. *J. Appl. Polym. Sci.* **2008**, *107*, 891–897. [CrossRef]
59. Santana Gomes, A.; Silva Simplicio, S.; Marinheiro da Cunha Gonsalves, J.K. Chitosan Nanoparticles as a Potential Drug Delivery System in the Skin: A Systematic Review Based on In Vivo Studies. *ChemistrySelect* **2024**, *9*, e202402058. [CrossRef]
60. Mahmud, T.H.T.; Abdul-Aziz, A.; Muda, R. A Review on the Potential Use of Chitosan-Based Delivery System in Mild Facial Cleansing Formulation. *Int. J. Polym. Mater. Polym. Biomater.* **2015**, *64*, 432–437. [CrossRef]
61. Wadhwa, K.; Kadian, V.; Puri, V.; Bhardwaj, B.Y.; Sharma, A.; Pahwa, R.; Rao, R.; Gupta, M.; Singh, I. New Insights into Quercetin Nanoformulations for Topical Delivery. *Phytomed. Plus* **2022**, *2*, 100257. [CrossRef]
62. Shah, J.; Patel, D.; Rananavare, D.; Hudson, D.; Tran, M.; Schloss, R.; Langrana, N.; Berthiaume, F.; Kumar, S. Recent Advancements in Chitosan-Based Biomaterials for Wound Healing. *J. Funct. Biomater.* **2025**, *16*, 45. [CrossRef]
63. Boots, A.W.; Haenen, G.R.M.M.; Bast, A. Health Effects of Quercetin: From Antioxidant to Nutraceutical. *Eur. J. Pharmacol.* **2008**, *585*, 325–337. [CrossRef]
64. Zagrean-Tuza, C.; Mot, A.C.; Chmiel, T.; Bende, A.; Turcu, I. Sugar Matters: Sugar Moieties as Reactivity-Tuning Factors in Quercetin O-Glycosides. *Food Funct.* **2020**, *11*, 5293–5307. [CrossRef]
65. Zielińska, D.; Starowicz, M.; Wronkowska, M.; Zieliński, H. Multifaceted Biological Activity of Rutin, Quercetin, and Quercetin's Glucosides. *Molecules* **2025**, *30*, 2555. [CrossRef]
66. Alves, T.F.R.; Morsink, M.; Batain, F.; Chaud, M.V.; Almeida, T.; Fernandes, D.A.; da Silva, C.F.; Souto, E.B.; Severino, P. Applications of Natural, Semi-Synthetic, and Synthetic Polymers in Cosmetic Formulations. *Cosmetics* **2020**, *7*, 75. [CrossRef]
67. Wang, Y.; Chen, S.; Yao, Y.; Wu, N.; Xu, M.; Yin, Z.; Zhao, Y.; Tu, Y. Effects of Citric Acid Crosslinking on the Structure and Properties of Ovotransferrin and Chitosan Composite Films. *Int. J. Biol. Macromol.* **2023**, *229*, 268–281. [CrossRef]